Rock and Soil Mechanics

Volume 42 | Issue 9 Article 2

12-14-2021

Prediction of unsaturated permeability curve of compaction loess with pore-size distribution curve and its application scope

Yan LI
Observation and Research Station of Water Cycle and Geological Environment for the Chinese Loess Plateau, Ministry of Education, Zhengning, Gansu 745399, China

Tong-lu LI
Observation and Research Station of Water Cycle and Geological Environment for the Chinese Loess Plateau, Ministry of Education, Zhengning, Gansu 745399, China, dcdgx08@chd.edu.cn

Xiao-kun HOU
Institute of Geology and Geophysics, Chinese Academy of Sciences, Beijing 100029, China

Hua LI
School of Equipment Management and Support, Armed Police Force Engineering University, Xi'an, Shaanxi 710086, China

See next page for additional authors

Custom Citation

LI Yan, LI Tong-lu, HOU Xiao-kun, LI Hua, ZHANG Jie, . Prediction of unsaturated permeability curve of compaction loess with pore-size distribution curve and its application scope[J]. Rock and Soil Mechanics, 2021, 42(9): 2395-2404.

Prediction of unsaturated permeability curve of compaction loess with pore-size distribution curve and its application scope

Authors
Yan LI, Tong-lu LI, Xiao-kun HOU, Hua LI, and Jie ZHANG

Rock and Soil Mechanics 2021 42(9): 2395−2404 ISSN 1000−7598
https: //doi.org/10.16285/j.rsm.2021.5277 rocksoilmech.researchcommons.org/journal

Prediction of unsaturated permeability curve of compaction loess with pore-size distribution curve and its application scope

LI Yan[1, 2], LI Tong-lu[1, 2], HOU Xiao-kun[3], LI Hua[4], ZHANG Jie[1, 2]

1. School of Geology Engineering and Surveying, Chang'an University, Xi'an, Shaanxi 710054, China
2. Observation and Research Station of Water Cycle and Geological Environment for the Chinese Loess Plateau, Ministry of Education, Zhengning, Gansu 745399, China
3. Institute of Geology and Geophysics, Chinese Academy of Sciences, Beijing 100029, China
4. School of Equipment Management and Support, Armed Police Force Engineering University, Xi'an, Shaanxi 710086, China

Abstract: The unsaturated permeability curve is governed by the pore-size distribution curve, which can be used to predict the permeability curve. In order to investigate the applicability of this method for compacted loess, three groups of compacted loess samples with different dry densities were prepared. The pore-size distribution (PSD) curves of soil samples were measured using mercury injection porosimeter test. The unsaturated permeability curves of soil samples were measured by small soil column equipment designed by our research group. Then the PSD curves were used to predict the permeability curves and compared with the measured data from soil column test. The results show that the permeability curves of compacted loess can be divided into a low matric suction stage dominated by capillary water, and a high matric suction stage dominated by adsorbed water. In the low suction stage, the permeability curves of the three soil samples differ greatly. While in the high suction section, the permeability curves of the three soil samples coincide, indicating that the permeability of the high suction section has nothing to do with the density of soil. In addition, the predicted results of three groups of soil samples are in good agreement with the measured data in the low suction section, but the predicted results in the high suction section are smaller than the measured results. It can be seen from the principle of the prediction method that this method is suitable for capillary water but not for adsorbed water. Therefore, a modified method is proposed for the prediction of permeability curve in the high suction section, and the modified method can describe the permeability curve in the whole matric suction range.

Keywords: compacted loess soil; instantaneous profile method; pore-size distribution curve; unsaturated permeability curve; prediction method

1 Introduction

Due to surface water infiltration, such as rainfall and artificial impounding, the degree of saturation of compacted loess increases, while the suction and the soil strength decrease, leading to a series of engineering problems including slope instability[1], collapsible deformation[2], post−construction settlement[3] and other problems. These geological phenomena are closely related to the permeability characteristics of unsaturated loess, and the permeability of unsaturated soil is described by the unsaturated permeability curve, which is a basic parameter reflecting the permeability of unsaturated soil[4−5].

The unsaturated soil permeability curve can be directly measured, as unsaturated permeability coefficient varies with the matric suction or water content. Current test methods, each with its own peculiarities, are all based on the principles of the steady-state method and the transient method[6−8], focusing on the measurement of matric suction. For example, Shao et al.[9] improved the pressure plate instrument to control the matric suction at both ends of soil sample to obtain the hydraulic gradient. In addition to measuring the permeability curve, Shao's method can also be used to measure the soil−water characteristic curve (SWCC), but the measurement range of matric suction is limited to the air-entry value of ceramic disk. Moreover, tensiometers, water potentiometers and other instruments are used to measure the suction of soil columns in water infiltration[10−11]. However, these methods require a large soil column sample, and the matric suction range is limited, not exceeding 100 kPa.

In view of the complexity and time-consuming process of the unsaturated soil permeability curve testing, many scholars have proposed models that can indirectly predict the permeability curve. The commonly used ones include Gardner's model[12], Childs and Collis-George's model[13] and van Genuchten's model[14]. The parameters in these prediction models are the same as SWCC, so SWCC has to be measured first. Recently, some researchers have proposed to establish prediction models from the micro perspective. Tao et al.[15] established the relationship between the permeability coefficient and the equivalent

Received: 22 February 2021 Revised: 8 May 2021
This work was supported by the National Natural Science Foundation of China(41790442, 41772278).
First author: LI Yan, female, born in 1997, Master, mainly engaged in the research of unsaturated loess and slope engineering. E-mail: liyan_dzgc@chd.edu.cn
Corresponding author: LI Tong-lu, male, born in 1965, PhD, Professor, mainly engaged in the research of geological disaster and unsaturated loess. E-mail: dcdgx08@chd.edu.cn

pore-size of micro pore channel, and deduced the equation of matric suction versus permeability coefficient, which was still based on SWCC. On the other hand, Zhang et al.[16] used the geometric relationship between soil particles and pores to determine the pore characteristics of the soil by the particle size distribution curve, and predicted the unsaturated permeability curve with the pore characteristics. This method has practical significance as it uses the more easily measured particle size distribution curve instead of the SWCC with more complex test steps. In addition, Romero et al.[17] directly predicted the permeability curve of Boom clay using the pore-size distribution (PSD) curve measured by the mercury injection instrument, which made the prediction of the permeability curve easier. However, their research results only verify the prediction of the method when the matric suction is less than 1 000 kPa, lacking unsaturated permeability coefficient in the range of high matric suction. Nevertheless, loess in arid-semi-arid region has low natural water content and high matric suction in shallow loess under the influence of rainfall and evaporation. Therefore, the hydraulic properties of unsaturated loess at high matric suction are also important, and its prediction methods and permeability characteristics need to be studied.

To better understand the permeability characteristics of unsaturated loess in the full suction range, especially in the high suction range, three sets of compacted loess samples are prepared in this research, the PSD curves and the unsaturated permeability coefficients are then measured in the full suction range of each soil sample by the mercury injection apparatus and the small soil column permeameter designed independently by our research group, respectively. Moreover, a method for predicting the permeability curve by PSD curve is developed and its application scope is discussed. Finally, the prediction method is modified by mechanism analysis to improve the applicability in the high matric suction range.

2 Methods

2.1 Sample preparation

The loess used for the preparation of compacted samples was taken from a natural slope on the south side of Xinyuan village in Hefangtai. Its natural water content is 8.0%, liquid limit is 26.5%, plastic limit is 17.4%, and plasticity index is 9.1, measured by indoor tests. Figure 1 shows the particle size distribution curves of the soil samples, indicating that the proportion of clay particles (<5 μm) is 14.6%, the proportion of silt particles (5−75 μm) is 74.9% and the proportion of sand particles (>75 μm) is 10.5%. According to *the standard for engineering classification of soil* (GB/T50145−2007)[18], the soil belongs to the low liquid limit clay.

From the compaction curve of soil samples, it is observed that the maximum dry density of the test material is 1.71 g /cm^3, and the optimum water content is 17.0%. In order to prepare the compacted soil samples with different structures[19], three kinds of soils with different water contents were prepared, namely, dry of optimum (8.0%), optimum (17.0%) and wet of optimum (19.0%). Compacted soil samples were prepared according to the compaction curve named A08, B17 and C19, respectively. The position of compacted soil samples on the compaction curve is shown in Fig.2, and their basic physical properties are summarized in Table 1.

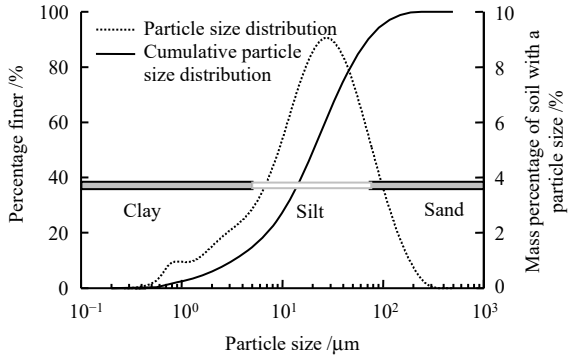

Fig. 1 Particle size distributions of soil samples

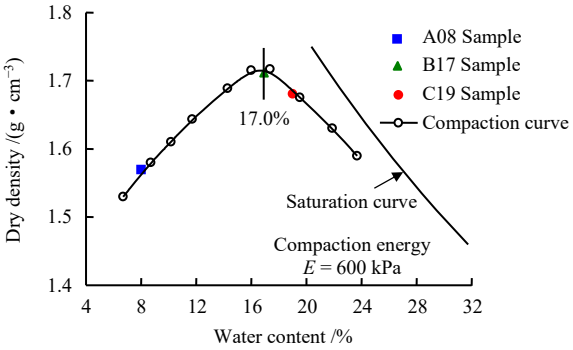

Fig. 2 Compaction curves of soil samples

Table 1 Physical properties of the compacted soils

Sample name	Water content /%	Specific gravity	Dry density /(g • cm^{-3})	Void ratio e	Actual porosity n_0 /%	Saturated permeability /(m • s^{-1})
A08	8.0	2.71	1.57	0.72	41.8	5.23×10^{-8}
B17	17.0	2.71	1.71	0.58	36.7	1.61×10^{-8}
C19	19.0	2.71	1.68	0.61	38.0	2.06×10^{-8}

2.2 Pore-size distribution curve measurement

Mercury injection porosimeter (MIP) test is one of the effective methods to determine the pore size, pore distribution and porosity of soil. The mercury as a non-wettable liquid can only overcome the surface tension and intrude into the soil pores under the action of external pressure. The mercury enters the large pores first and then the small pores with the increase of the intrusion pressure

applied to the mercury. The relationship between the pore size and the mercury intrusion pressure is converted by Washburn's formula as follows[20]:

$$P_{\mathrm{Hg}} = -\frac{4T_{\mathrm{Hg}}\cos\alpha_{\mathrm{m}}}{D} \tag{1}$$

where P_{Hg} is the mercury intrusion pressure; D is the pore diameter corresponding to the mercury intrusion pressure P_{Hg}; T_{Hg} is the surface tension of mercury, which is 0.485 N /m at 20 °C; α_{m} is the contact angle between mercury and soil particles, which is commonly regarded as a constant value and is taken as 130º [21−22] or 140º [23] In this paper, it was set as 130º.

The AutoPore IV 9500 mercury injection instrument was used for the MIP test, with a low intrusion pressure range of 3−207 kPa and a high intrusion pressure range of 207−413 700 kPa. It can be used to determine the pore diameter of 0.003−345 μm. During the test, the ambient temperature was controlled at 20(±2) ℃ by setting the air conditioner to 20 ℃. At the same time, good ventilation conditions should be maintained. Before the test, the cubes of 10 mm×10 mm×10 mm were cut from the compacted samples, freeze-dried and weighed. Then, the cube sample was placed horizontally in the dilatometer and vacuumized. After vacuumizing, the mercury was injected into the dilatometer and the pressure was gradually applied to make the mercury enter the pores of the sample. The mercury injection instrument can automatically record the mercury intrusion pressure P_{Hg}, the mercury intrusion volume ΔV and the cumulative mercury intrusion volume V under the pressure P_{Hg}, and measure the total porosity of soil n_{t} in the meantime. The pore diameter D corresponding to P_{Hg} can be calculated using Eq.(1), and the relationship between pore diameter D and cumulative mercury intrusion volume V can be obtained.

2.3 Permeability measurement

The saturated permeability coefficient was tested by falling head method with TST-55 permeameter and the unsaturated permeability coefficient was determined by a small soil column permeameter designed independently by our research group[24]. Figure 3 presents the installation diagram of the small soil column permeameter. The equipment includes two parts: the water supply system and the soil column. The water supply system consists of a water supply bottle, a Mariotte bottle and a low-permeability porous stone, which can supply water to the soil column at a steady flow rate under the constant water head. The soil column is composed of 6 dried ring-cut soil samples and 5 dried suction-measuring filter papers. Each soil sample is covered with ordinary filter papers at the top and bottom surfaces so that the suction-measuring filter paper sandwiched in the middle is not contaminated and the soil sample is prevented from falling. During the test, the water supply system is placed above the soil column to make sure the water infiltration in the soil column, and the mass of each soil sample and the suction-measuring filter paper need to be weighed every 4 hours.

Whatman No. 42 filter paper was used as the suction-measuring paper in the test, whose matric suction can be calculated by a conversion from mass water content using the calibration equation provided by ASTM as follows[25]:

$$\lg\psi = \begin{cases} 5.327 - 0.077\,9w_{\mathrm{fp}}\ , & w_{\mathrm{fp}} < 45.3\% \\ 2.412 - 0.013\,5w_{\mathrm{fp}}\ , & w_{\mathrm{fp}} \geqslant 45.3\% \end{cases} \tag{2}$$

where ψ is the matric suction of soil samples; w_{fp} is the mass water content of the suction-measuring filter paper.

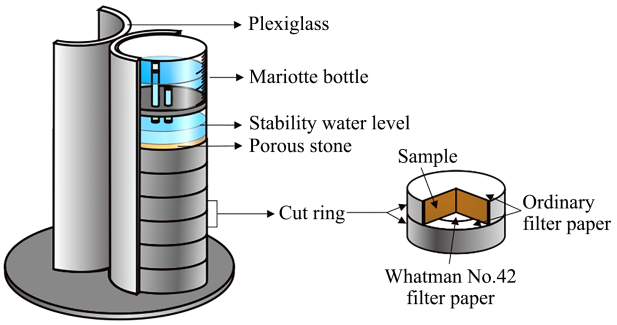

Fig. 3 Installation diagram of small soil column permeameter

Figure 4 shows the distribution of total water head and water content at different moments. The calculation method of unsaturated permeability coefficient is introduced by taking the arbitrary calculated m section as an example. The total height of the soil column is 12 cm and if the depth of m section, z_m, is equal to 8 cm, so z_{m-1} represents the upper calculated section depth, z_{m-1} = 6 cm. Then, the average velocity $v_{zm,\,t\mathrm{ave}}$ of water flow through the m section during the time period t_1 to t_2 is calculated by the following formula:

$$v_{zm,\,t\,\mathrm{ave}} = \frac{\mathrm{d}}{\mathrm{d}t}\int_{z_{\mathrm{L}}}^{z_m}\theta_{\mathrm{w}}(z,t)\,\mathrm{d}z \approx \frac{\Delta V_{\mathrm{w}}}{A(t_2 - t_1)} \tag{3}$$

where $\theta_{\mathrm{w}}(z,t)$ is the function of volume water content with respect to depth z at time t; ΔV_{w} is the volume of water flowing through m section from time t_1 to t_2, i.e. area of the shaded part in Fig.4; dt is the measured time interval, i.e. t_2-t_1; A is the cross-sectional area of soil column; and z_{L} is the coordinate of the bottom surface of the soil column, i.e. the height of the soil column is 12 cm.

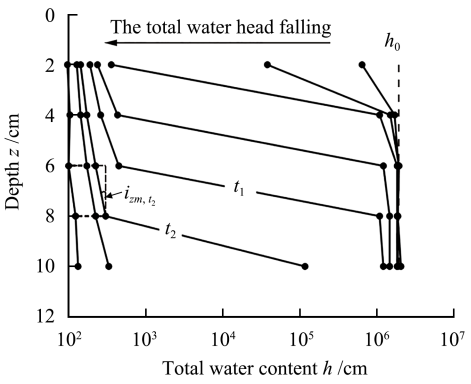

(a) Water head

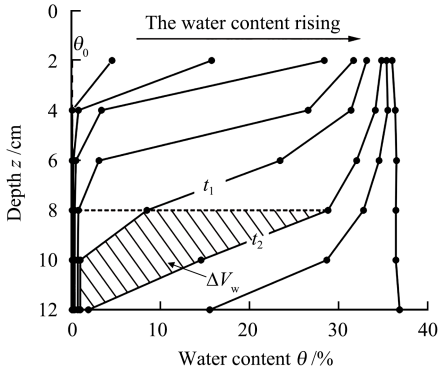

(b) Water content

Note: each curve in the figure is the total water head (or water content) measured at the bottom of the ring-cut samples at different moments in the soil column test, h_0 and θ_0 are the initial total water head and the initial water content, $i_{zm,t_2}=\frac{h_{zm,t_2}-h_{zm-1,t_2}}{z_m-z_{m-1}}$

Fig. 4 Distribution of water head and water content at different positions of soil column at different moments

As shown in Fig.4, the hydraulic gradient of m section at time t_2 is i_{zm,t_2}, and the hydraulic gradient at time t_1 is i_{zm,t_1}, then the average hydraulic gradient ($i_{zm,t\text{ave}}$) within Δt at m section can be calculated by backward differential method:

$$i_{zm,t\text{ave}}=\frac{1}{2}\left(\frac{h_{zm,t_2}-h_{zm-1,t_2}}{z_m-z_{m-1}}+\frac{h_{zm,t_1}-h_{zm-1,t_1}}{z_m-z_{m-1}}\right) \quad (4)$$

where h_{zm,t_1} and h_{zm,t_2} are the total water head of m section at time t_1 and t_2, respectively; h_{zm-1,t_1} and h_{zm-1,t_2} are the total water head at $m-1$ section at time t_1 and t_2, respectively.

The unsaturated permeability coefficient k_m of m section within Δt is calculated by the Darcy's law, and the corresponding matric suction ψ is the average matric suction of the suction-measuring filter paper of m section within t_1 and t_2. k_m is

$$k_m=-\frac{v_{zm,t\text{ave}}}{i_{zm,t\text{ave}}} \quad (5)$$

3 Interpretation of the experimental results

3.1 Pore-size distribution curve

The cumulative pore-size distribution curves of compacted soil samples measured by MIP test and further calculated pore-size density distribution curves are collectively referred to as pore distribution curves, or PSD curves, as shown in Fig.5. Fig.5(a) is the curve that shows the relation between pore diameter D of compacted soil samples and cumulative mercury intrusion porosity n_{in}. n_{in} is obtained by converting the total porosity n_{t}, the cumulative mercury intrusion volume V and total mercury intrusion volume V_{t} measured by the AutoPore IV 9500 mercury injection instrument, i.e. $n_{\text{in}}=(n_{\text{t}}V)/V_{\text{t}}$. The total porosities of compacted samples A08, B17 and C19 are 36.5%, 32.0% and 34.3%, respectively. However, the actual porosity n_0 of the specimens are 41.8%, 36.7% and 38.0% (see Fig.5). It can be noted that the total porosity measured by the MIP test is slightly smaller than the actual porosity, by approximately 10%. One reason for this slight difference is that the mercury can only enter the interconnected pore channels under the action of external forces, but not the pores which are closed. There is another fact that the pore diameter measurement range of the MIP test is limited to the range of 0.003−345 μm. Therefore, the total porosity n_{t} measured by the MIP test is smaller than the actual porosity n_0. When using the PSD curves to calculate the permeability curves, only the influence of interconnected pores on the unsaturated permeability is considered, so the error between the total porosity n_{t} and the actual porosity n_0 can be ignored. Fig.5(b) shows the pore-size density distribution curves of the compacted samples, which are the derivation of the cumulative pore-size distribution curves. Since the cumulative distribution curve has a large pore diameter range, it is more straightforward to plot in logarithmic coordinate, so the derivation should also be considered in logarithmic coordinate, that is, the y-axis corresponding to the pore-size density distribution curve is $-\text{d}V/\text{dlg}D$. The PSD curves of the three compacted soil sample groups show that the pore-size distributions are in good agreement with macro parameters. In general, A08 has the smallest dry density and the largest void ratio, so its PSD curve has a very sharp single peak and a narrow pore-size range, with the dominant pore size at around 3.6 μm. On the contrary, B17 has the highest dry density and the lowest void ratio, and C19 has a smaller dry density and a higher void ratio than that of B17, but they are close to each other. Therefore, the PSD curves of both are similar with a low peak and a wide range, indicating a more uniform pore-size distribution, and compared to A08, they have fewer large pores and more small pores. The pore-size

density distribution curves of the three compacted samples are significantly different in the pore diameter range of 0.2−10 μm. Beyond this range the pore-size density curves basically overlapped, suggesting that the compaction process mainly occurred in the pores of 0.2−10 μm. There are few pores with the diameter greater than 10 μm in the samples, and the pore-size density distribution curve is close to the *x*-axis. When the pore diameter is less than 0.2 μm, the cumulative pore-size distribution curves of the three samples are similar, and the pore-size density distribution curves coincide, that is, the pore-size distributions of the compacted samples are similar when the pore size is less than 0.2 μm, indicating that the pore diameter in this range does not change during the compaction process.

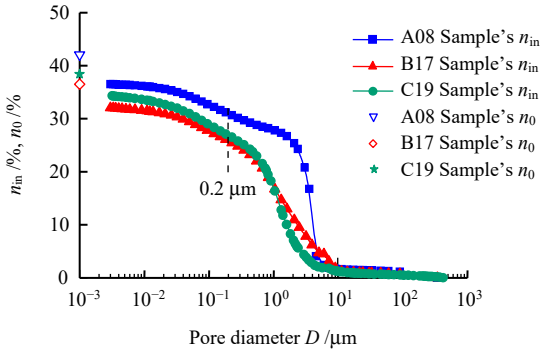

(a) Cumulative pore-size distribution curve

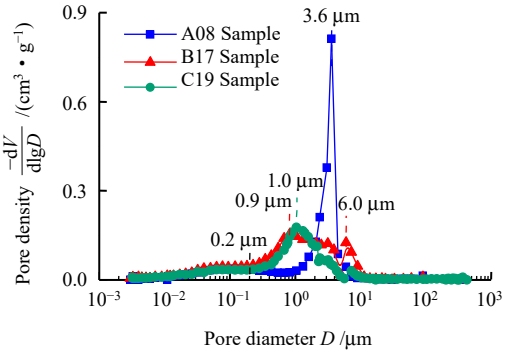

(b) Pore-size density distribution curve

Fig. 5 Pore-size distribution curves of the compacted samples

3.2 Measured permeability coefficient

Table 1 shows the saturated permeability coefficient measured by the falling-head test, which can be seen to correspond to the void ratio and dry density.

The unsaturated permeability coefficient k_m corresponding to different matric suction ψ was obtained by calculating the small soil column test results according to the method in section 2.3, as shown in the scatter points in Fig.6. It can be observed that the matric suction of the compacted samples is tested in the range of 3−10^5 kPa, and the unsaturated permeability coefficient varies from 10^{-15} m /s to 10^{-8} m /s, up to 7 orders of magnitude. The characteristics of the permeability curve show that when the matric suction is less than 10 kPa, the unsaturated permeability coefficient of compacted samples increases at a lower rate as the matric suction decreases, and the permeability curve becomes almost horizontal. As the logarithmic coordinate cannot be set to 0, the permeability coefficient corresponding to the matric suction of 1 kPa is taken as the saturated permeability coefficient measured in the falling head test and marked with a solid pattern in Fig.6.

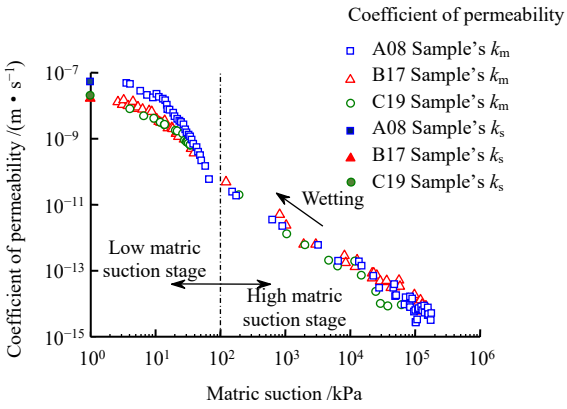

Fig. 6 Scatter diagram of measured unsaturated permeability coefficient of compacted samples

As can be seen from the measured results, the unsaturated permeability coefficient can be divided into two stages bounded by the matric suction of 100 kPa. In the high matric suction stage (>100 kPa), the unsaturated permeability coefficients of three samples basically overlap and roughly show an oblique line in the log-logarithmic coordinate system, which elucidates that the permeability of compacted samples in the high matric suction stage is independent of the dry density. In the low matric suction stage (<100 kPa), the unsaturated permeability coefficients of three samples differ significantly: A08 has the smallest dry density and more large pores, so the unsaturated permeability coefficients at the same matric suction are higher than those of the other two soil samples; while B17 and C19 have the similar dry density and PSD curves, their measured unsaturated permeability coefficients are also similar.

4 Predicting permeability curve with PSD curve

Firstly, the pore-size distribution function $F(D)$ and the density function $f(D)$ of the soil sample are obtained by quantitatively expressing the pore distribution characteristics of the compacted sample according to the PSD curve:

$$F(D)=1-\frac{V}{V_t} \tag{6}$$

$$f(D)=\frac{\mathrm{d}F(D)}{\mathrm{d}D}=-\frac{1}{V_t}\frac{\mathrm{d}V}{\mathrm{d}D}=-\frac{1}{V_t}\frac{1}{D\ln 10}\frac{\mathrm{d}V}{\mathrm{d}\lg D} \tag{7}$$

$-\mathrm{d}V/\mathrm{d}\lg D$ is the same as in Fig.5(b). When $D=D_{\min}$, $F(D_{\min})=0$, when $D=D_{\max}$, $F(D_{\max})=1$, and $\int_{D_{\min}}^{D_{\max}} f(D)\mathrm{d}D=1$. $D_{\min}$, $D_{\max}$ are the minimum and maximum pore diameters, respectively.

It is assumed that the soil pores are a series of parallel cylindrical pore channels. Their size and distribution are determined by the density function $f(D)$. $f(D)\mathrm{d}D$ is defined as the water content $\mathrm{d}\theta$ for the pores with diameter D–$D+\mathrm{d}D$ to be filled with water[26]:

$$\mathrm{d}\theta(D)=f(D)\mathrm{d}D \tag{8}$$

When the matric suction is high, water occupies the small pores first, and with the decrease of matric suction, water gradually occupies large pores. Given the matric suction ψ, only the pores with diameter less than D are filled with water, and the relationship between D and ψ is calculated by the Yang-Laplace equation[27]:

$$\psi=-\frac{4T_s\cos\alpha_w}{D} \tag{9}$$

where T_s is the surface tension of water. It is taken to be 72.75×10^{-3} N/m for free water at 20 °C; α_w is the contact angle between water and soil particles, and is taken to be 75°[28].

The Hagen-Poiseuille equation[29] provides a formula for calculating the average velocity v of liquid in laminar flow in a cylindrical channel with diameter D:

$$v=\frac{\rho_w g D^2 i}{32\mu} \tag{10}$$

where μ is the dynamic viscosity coefficient; g is the acceleration of gravity; ρ_w is the density of water; and i is the hydraulic gradient.

At a given matric suction, only the pore channels with pore diameter less than D are filled with water. Combining Eqs. (8) and (10) to calculate the corresponding flow rate $\mathrm{d}q$ at a water content increment $\mathrm{d}\theta$, the total flow rate per unit time is calculated by the following equation:

$$q(D)=\int_{D_{\min}}^{D}\mathrm{d}q(D)=\int_{D_{\min}}^{D}v\,\mathrm{d}\theta(D)=$$

$$\frac{\rho_w g i}{32\mu}\int_{D_{\min}}^{D}D^2 f(D)\mathrm{d}D \tag{11}$$

The water flow in the laminar state satisfies Darcy's law, and the unsaturated permeability coefficient corresponding to pore diameter D is

$$k(D)=\frac{\rho_w g}{32\mu}\int_{D_{\min}}^{D}D^2 f(D)\mathrm{d}D \tag{12}$$

All pores are filled with water when the soil reaches the saturation permeability coefficient, i.e.

$$k(D_{\max})=\frac{\rho_w g}{32\mu}\int_{D_{\min}}^{D_{\max}}D^2 f(D)\mathrm{d}D \tag{13}$$

Therefore, the unsaturated permeability coefficient $k_w(D)$ can be obtained from the definition of the relative permeability coefficient as the saturated permeability coefficient k_s of the soil is known, i.e.

$$k_w(D)=k_s\frac{\int_{D_{\min}}^{D}D^2 f(D)\mathrm{d}D}{\int_{D_{\min}}^{D_{\max}}D^2 f(D)\mathrm{d}D} \tag{14}$$

The results of the MIP test are used to classify the pores of the soil into N classes according to their diameter. D_l represents the pore diameter corresponding to the lth pore class, $1<l<N$, and ΔD_l represents the difference of pore diameter between the lth pore class and the $(l-1)$th pore class. When $l=1$ and $l=N$, D_l represents the smallest pore diameter $D_{\min}$ and the largest pore diameter $D_{\max}$, respectively, and when $l=j$, D_l represents any pore diameter D_j. The unsaturated permeability coefficient corresponding to D_j can be written as the summation form:

$$k_w(D_j)\approx k_s\frac{\sum_{l=1}^{j}D_l^2 f(D_l)\Delta D_l}{\sum_{l=1}^{N}D_l^2 f(D_l)\Delta D_l} \tag{15}$$

The relationship between the unsaturated permeability coefficient and pore diameter is first calculated from Eq.(14) or Eq.(15); and then the pore diameter is converted to matric suction from Eq.(9) to obtain the relationship between the predicted permeability coefficient and matric suction.

The pore-size density distribution data measured in the MIP test (Fig.5(b)) is substituted into Eqs. (7) and (15), and the pore diameter is converted into matric suction to obtain the predicted values of the permeability curve of the compacted samples, which is plotted in Fig.7. By comparing the measured and predicted data of the three compacted samples in Fig.7, it can be seen that the predicted data in the low suction stage are in good agreement with the measured data points; while the predicted results in the high suction section deviate systematically from the measured data, and the higher

the suction, the larger the deviation, which reflects that the PSD curve prediction method for unsaturated permeability is not applicable to the compacted loess in the high suction stage. For this kind of compacted loess, the range of the predictability is between 0−100 kPa, and beyond 100 kPa, the prediction effect decreases significantly as the matric suction increases.

The main reasons why the prediction curve matches with the measured data in the low matric suction stage, while deviates from the measured data in the high suction stage are that the action property of soil particles on water varies in different stages, and the occurrence form of pore water also changes. The prediction method with PSD curve is established based on the Hagen-Poiseuille equation[29] for capillary water. The surface tension T_s in Eq.(9), the water density ρ_w and the dynamic viscosity coefficient μ in Eq.(10) are all measured in free water and taken as constant values. These values are basically realistic in the low matric suction stage, such as the connected capillary water shown in Fig.8(a). When the suction increases, the surface tension, density and dynamic viscosity coefficient of water are no longer constant, they will increase as the matric suction rises, causing the predicted value to systematically deviate from the measured data.

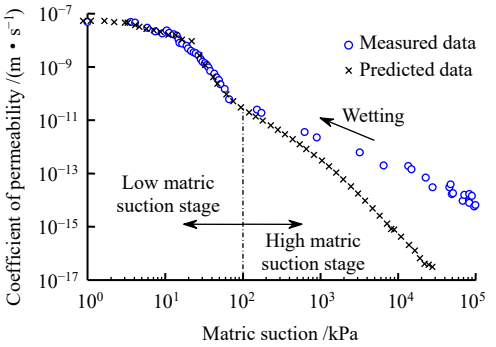

(a) A08 Sample

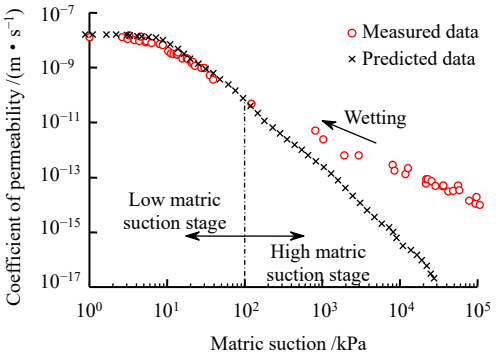

(b) B17 Sample

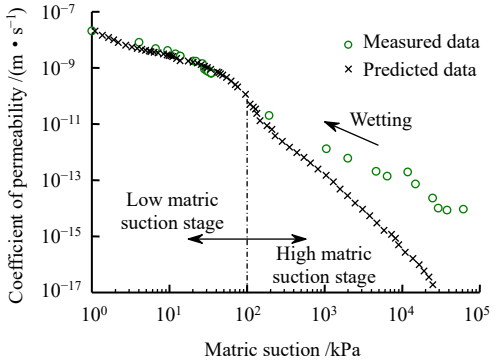

(c) C19 Sample

Fig. 7 Comparison of measured and predicted unsaturated permeability coefficients of compacted samples

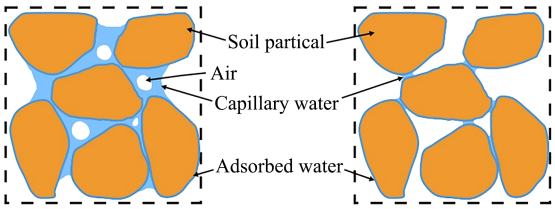

(a) Low matric suction stage (b) High matric suction stage

Fig. 8 Occurrence form of pore water in different matric suction stages

In addition to the influences of surface tension, density and dynamic viscosity coefficient of pore water, the unsaturated permeability coefficient in the high matric suction stage is also related to the thin film flow[30−31]. As shown in Fig.8(b), water in the high matric suction stage is adsorbed on the surface of soil particles to form the adsorbed water. The adsorbed water migrates on the surface of soil particles in the form of thin film flow, and its flow rate is positively correlated with film thickness and water content[30]. The higher the soil water content, the thicker the thin film on the soil particle surface, the smaller the adsorption force of water molecules, and the faster the migration speed of pore water driven by gravity and suction head. The measured data in this paper also show that the unsaturated permeability increases slowly with the decrease of matric suction in the high matric suction stage. Zhang et al.[31] calculated the saturated permeability coefficient of thin film flow on the silt particles surface as about 1.6×10^{-12} m /s using the average particle size and porosity of silt, which is much smaller than the saturated permeability of silt soil itself, indicating that the thin film flow contributes less to the soil seepage and can be neglected when the soil is close to saturation or at the stage of low matric suction. However, in the high matric suction stage, when only capillary flow is considered and the influence of film flow on permeability coefficient is ignored, the predicted result will be much smaller than the measured data. Therefore, a distinction should be made between capillary water and adsorbed water when describing and predicting the permeability characteristics of unsaturated soils.

Baker et al.[32] believed that the capillary water of soil is affected by atmospheric pressure, and its tension has a limit value ψ_c, called cavitation tension. When the matric suction is greater than this value, the capillary water is vaporized, and only adsorbed water is available in the soil[33], which is controlled by the adsorption on the soil particle surface. In addition, at this time, the adsorption strength is a single value function of water content, independent of dry density. Baker et al.[32] also concluded from the data in the literatures that the cavitation tension of pore water in soil is between 80 and 400 kPa, and the smaller soil particle size has the greater the cavitation tension. For instance, 80 kPa for most sand and 400 kPa for some clay. Lu et al.[34] also pointed out that the suction range of capillary water in unsaturated soil is 0−100 kPa, and the suction range of adsorbed water is 100−10^6 kPa. These experimental results are in agreement with the compacted loess in this paper. As can be seen from Fig.6, the ψ_c value of the compacted samples measured in this paper is about 100 kPa, the unsaturated permeability curves of the three compacted samples overlap when the matric suction is greater than 100 kPa and are independent of the dry density. This interesting result implies that the pore-size distribution and dry density can be ignored for the compacted loess when the matric suction is greater than 100 kPa. Furthermore, the unsaturated permeability curve is a straight line in the log-logarithmic coordinate system. Therefore, the measured data in the high matric suction stage is fitted with a power function and it is used to calibrate the unsaturated permeability curve of high suction range for prediction purposes:

$$k_w = a\psi^c \tag{16}$$

where c and a are the calibration parameters. This prediction method is suitable for different compacted soil samples made from loess with the same particle size composition.

For the permeability curve in the low suction section, the Gardner equation[12] is used to fit the prediction data points to obtain a smooth prediction curve

$$k_w = \frac{k_s}{1+(b\psi)^n} \tag{17}$$

where n and b are the fitting parameters.

The parameter ω is then introduced to represent the contribution of adsorption to the unsaturated permeability coefficient. When $\psi>\psi_c$, adsorption dominates and ω = 1; when $\psi<\psi_c$, capillarity dominates and $\omega = 0$. Combining Eq.(16) and Eq.(17) to obtain the expression for the permeability curve used to describe the full matric suction range:

$$k_w(\psi) = \left[\frac{k_s}{1+(b\psi)^n}\right]^{1-\omega} k_w(\psi_c)^{\omega}\left(\frac{\psi}{\psi_c}\right)^{\omega c} \tag{18}$$

Based on the results of the measured data, the data with matric suction greater than ψ_c is firstly fitted with Eq.(16), as shown in Fig.9, to determine the parameters c and a. Then the unsaturated permeability coefficient $k_w(\psi_c)$ corresponding to ψ_c is calculated by substituting Eq.(16). Next, the predicted data within the low matric suction stage are fitted by Eq.(17) to determine the parameters k_s, b and n, and the fitted parameters are shown in Table 2. Finally, the predicted permeability curve is corrected by Eq.(18), and the corrected permeability curve with the measured data are plotted in Fig.10, which demonstrates that the revised method can characterize the permeability curve of compacted loess in the full suction range.

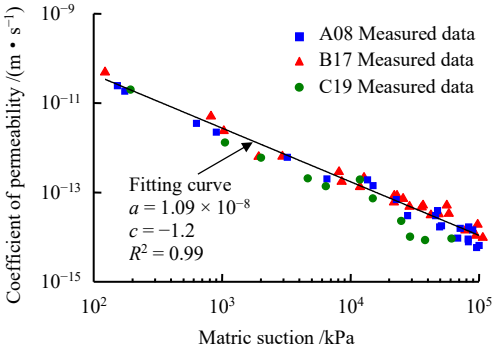

Fig. 9 Fitting curve of high matric suction stage of compacted samples

Table 2 Parameters of permeability curve

Sample name	ψ_c /kPa	$k_w(\psi_c)$ /(m • s^{-1})	Equation (17)		
			k_s /(m • s^{-1})	b	n
A08	100	4.36×10^{-11}	4.28×10^{-8}	0.09	3.20
B17	100	4.36×10^{-11}	1.31×10^{-8}	0.13	2.20
C19	100	4.36×10^{-11}	8.35×10^{-9}	0.11	2.21

The matric suction in the measured data is substituted into Eq.(18) to obtain the corresponding predicted unsaturated permeability coefficient which was compared with the measured unsaturated permeability coefficient, as shown in Fig.11. The determination coefficients R^2_{A08}, R^2_{B17}, R^2_{C19} between the predicted values and measured values of the three compacted samples are all higher than 0.90, indicating that the predicted and measured values are highly consistent, and the modified PSD curve prediction method can accurately predict the permeability curve within the full suction range of the compacted

loess.

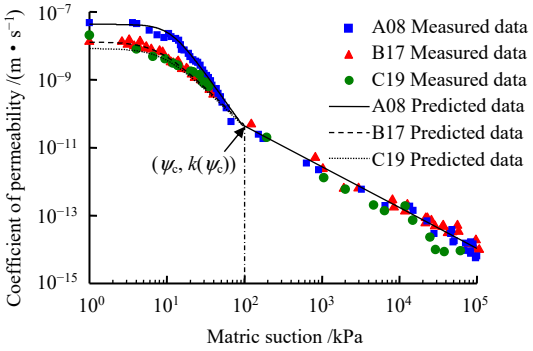

Fig. 10 Comparisons of modified predicted permeability curves and measured data

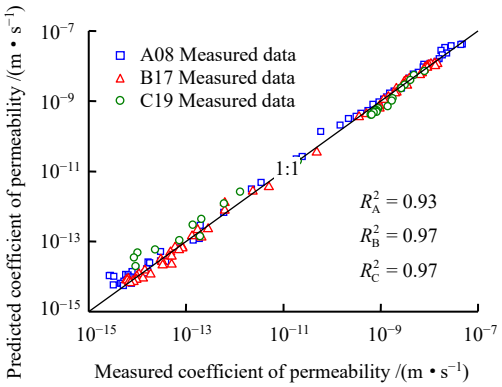

Fig. 11 Comparison between predicted and measured permeability coefficients

5 Conclusion

In this paper, three groups of compacted loess samples with different dry densities were chosen from the compaction curves with dry of optimum water content (8.0%), optimum water content (17.0%) and wet of optimum water content (19.0%). The pore-size distribution characteristics and unsaturated permeability curve characteristics of these compacted samples were analyzed. Then the pore distribution curves were also used to predict the permeability curves of compacted loess to explore the applicability of this prediction method, and the conclusions were drawn:

(1) The PSD curves of the three compacted sample groups differ greatly within the range of 0.2−10 μm. When the pore size is less than 0.2 μm, the pore distributions of compacted soil samples are similar, so the compaction process mainly occurs in the pores of 0.2−10 μm.

(2) 100 kPa is taken as a boundary, the permeability curves of compacted samples can be divided into two stages. The difference of permeability curves of compacted samples is mainly reflected in the low matric suction stage (lower than 100 kPa). While in the high matric suction stage (higher than 100 kPa), the permeability curves of the three compacted sample groups overlap and form an oblique straight line in the log-logarithmic coordinate system.

(3) The prediction method of the permeability curve with PSD curve is suitable for the compacted loess in the low matric suction stage, but the prediction results deviate from the measured data in the high matric suction stage. The measured data in the high matric suction stage can be used to calibrate the parameters and modified the prediction method. As a result, the modified method can be used to describe the permeability curve over the full suction range.

References

[1] HOU X K, VANAPALLI S K, LI T L. Water infiltration characteristics in loess associated with irrigation activities and its influence on the slope stability in Heifangtai loess highland, China[J]. Engineering Geology, 2018, 234: 27−37.

[2] FANG Jin-jin, FENG Yi-xin, YU Yong-qiang, et al. Wetting deformation characteristics of intact loess under true triaxial conditions[J]. Rock and Soil Mechanics, 2020, 41(4): 1235−1246.

[3] DU Wei-fei, ZHENG Jian-guo, LIU Zheng-hong, et al. Settlement behavior of high loess-filled foundation and impact from exhaust conditions[J]. Rock and Soil Mechanics, 2019, 40(1): 325−331.

[4] HOU X K, VANAPALLI S K, LI T L. Water flow in unsaturated soils subjected to multiple infiltration events[J]. Canadian Geotechnical Journal, 2020, 57(3): 366−376.

[5] NG C W W, LEUNG A K. Measurements of drying and wetting permeability functions using a new stress-controllable soil column[J]. Journal of Geotechnical and Geoenvironmental Engineering, 2012, 138(1): 58−68.

[6] LI Yong-le, LIU Cui-ran, LIU Hai-ning, et al. Testing study on permeability characteristics of unsaturated soil[J]. Chinese Journal of Rock Mechanics and Engineering, 2004, 23(22): 3861−3865.

[7] WANG Hong, LI Tong-lu, FU Yu-kai. Determining permeability function of unsaturated loess by using instantaneous profile method[J]. Journal of Hydraulic Engineering, 2014, 45(8): 997−1003.

[8] XU Yong-fu, LAN Shou-qi, SUN De-an, et al. New apparatus for measurement of stress effect on permeability of unsaturated soil[J]. Chinese Journal of Rock Mechanics and Engineering, 2005, 24(1): 160−164.

[9] SHAO Long-tan, WEN Tian-de, GUO Xiao-xia. Direct measurement method and prediction formula for permeability coefficient of unsaturated soils[J]. Chinese Journal of Geotechnical Engineering, 2019, 41(5): 806−812.

[10] ZHAN Liang-tong, HU Ying-tao, LIU Xiao-chuan, et al. Centrifuge modelling of rainfall infiltration in an unsaturated

loess and joint monitoring of multi-physical parameters[J]. Rock and Soil Mechanics, 2019, 40(7): 2478−2486.

[11] ZHANG Lin, ZHANG Deng-fei, CHEN Cun-li, et al. Experimental study on compression collapsibility and infiltration of remolded loess soil column under vertical pressure[J]. Journal of Hydraulic Engineering, 2019, 50(10): 1214−1221.

[12] GARDNER W R. Some steady solutions of the unsaturated moisture flow equation with application to evaporation from a water table[J]. Soil Science, 1958, 85(4): 228−232.

[13] CHILDS E C, COLLIS-GEORGE N. The permeability of porous materials[J]. Proceedings of the Royal Society of London, 1950, 201(1066): 392−405.

[14] VAN GENUCHTEN M T. A closed-form equation for predicting the hydraulic conductivity of unsaturated soils[J]. Soil Science Society of America Journal, 1980, 44(5): 892−898.

[15] TAO Gao-liang, KONG Ling-wei. A model for determining the permeability coefficient of saturated and unsaturated soils based on micro pore channel and its application[J]. Journal of Hydraulic Engineering, 2017, 48(6): 702−709.

[16] ZHANG Zhao, CHENG Jing-xuan, LIU Feng-yin, et al. Physical approach to predict unsaturated permeability function based on soil particle size distribution[J]. Rock and Soil Mechanics, 2019, 40(2): 549−560.

[17] ROMERO E, GENS A, LLORET A. Water permeability, water retention and microstructure of unsaturated compacted Boom clay[J]. Engineering Geology, 1999, 54(1-2): 117−127.

[18] Ministry of Water Resources of the People's Republic of China. GB/T 50145−2007 standard for engineering classification of soil[S]. Beijing: China Planning Publishing House, 2008.

[19] VANAPALLI S K, FREDLUND D G, PUFAHL D E. The Influence of soil structure and stress history on the soil-water characteristics of a compacted till[J]. Géotechnique, 1999, 51(6): 573−576.

[20] WASHBURN E W. Note on a method of determining the distribution of pore sizes in a porous material[J]. Proceedings of the National Academy of Sciences of the United States of America, 1921, 7(4): 115−116.

[21] WU Zhu-min, LÜ Qing-feng, WANG Sheng-xin. Microstructure of loess reinforced by compositely modified sodium silicate[J]. Rock and Soil Mechanics, 2016, 37(Suppl.2): 301−308.

[22] NIU Geng, SUN De-an, WEI Chang-fu, et al. Determination of water retention curve of fully weathered mudstone using its pore-size distribution[J]. Rock and Soil Mechanics, 2018, 39(4): 1337−1345.

[23] ZHANG Xian-wei, KONG Ling-wei, GUO Ai-guo, et al. Experiment study of pore distribution of strong structural clay under different consolidation pressures[J]. Rock and Soil Mechanics, 2014, 35(10): 2794−2800.

[24] LI Hua, LI Tong-lu, JIANG Run-jun, et al. Measurement of unsaturated permeability curve using filter paper method[J]. Rock and Soil Mechanics, 2020, 41(3): 895−904.

[25] ASTM International. D5298−10 Standard test method for measurement of soil potential (suction) using filter paper[S]. West Conshohocken: American Society for Testing and Materials, 2013.

[26] FREDLUND D G, XING A. Equations for the soil-water characteristic curve[J]. Canadian Geotechnical Journal, 1994, 31(4): 521−532.

[27] SIMMS P H, YANFUL E K. Predicting soil-water characteristic curves of compacted plastic soils from measured pore-size distribution[J]. Géotechnique, 2002, 52(4): 269−278.

[28] LI H, LI T L, LI P, et al. Prediction of loess soil-water characteristic curve by mercury intrusion porosimetry[J]. Journal of Mountain Science, 2020, 17(9): 2203−2213.

[29] SUTERA S P, SKALAK R. The history of Poiseuille's law[J]. Annual Review of Fluid Mechanics, 1993, 25(1): 1−20.

[30] TOKUNAGA TETSU K. Hydraulic properties of adsorbed water films in unsaturated porous media[J]. Water Resources Research, 2009, 45(6): 735−742.

[31] ZHANG Zhao, LIU Feng-yin, ZHANG Guo-ping. Models for water retention and unsaturated permeability in full range of water content[J]. Chinese Journal of Geotechnical Engineering, 2014, 36(11): 2069−2077.

[32] BAKER R, FRYDMAN S. Unsaturated soil mechanics: critical review of physical foundations[J]. Engineering Geology, 2009, 106(1-2): 26−39.

[33] XU Xiao, ZHAO Cheng-gang, CAI Gou-qing. Shear strength of unsaturated soils considering capillary and adsorptive mechanisms[J]. Rock and Soil Mechanics, 2018, 39(6): 2059-2064, 2072.

[34] LU N, LIKOS W J. Unsaturated soil mechanics[M]. Hoboken: John Wiley & Sons, Inc., 2004: 309−377.